

# Simulation Results of Arc Behavior in Different Plasma Spray Torches

*J. P. Trelles, J. V. R. Heberlein*

Department of Mechanical Engineering, University of Minnesota, Minneapolis, Minnesota,  
USA

## Abstract

Three-dimensional, transient simulations of the plasma flow inside different plasma spray torches have been performed using a local thermodynamic equilibrium model solved by a multiscale finite element method. The model describes the dynamics of the arc without any further assumption on the reattachment process except for the use of an artificially high electrical conductivity near the electrodes. Simulations of an F4-MB torch from Sulzer-Metco and two configurations of the SG-100 torch from Praxair are presented. The simulations show that, when straight or swirl injection is used, the arc is dragged by the flow and then jumps to form a new attachment, preferably at the opposite side of the original attachment, as has been observed experimentally. Although the predicted reattachment frequencies are at present higher than the experimental ones, the model is suitable as a design tool.

*Keywords:* plasma torch, arc dynamics, time-dependent, three-dimensional, multiscale finite elements

## Introduction

Better reproducibility of plasma spraying processes is one of the major goals in current research and development efforts in thermal plasma technology [1]. To achieve this goal, a better understanding of the dynamics of the arc inside direct current (DC) non-transferred arc plasma torches, as commonly used in plasma spraying, is required because the movement of the arc inside the torch has a first order effect on both: coating quality (due to the forcing of the jet, enhancing cold flow entrainment and non-uniform powder heating) and anode lifetime (due to the localized heating of the anode).

Figure 1 shows schematically the flow inside a DC plasma torch. The arc dynamics are a result of the balance between the drag force caused by the interaction of the incoming gas flow over the arc and the electromagnetic (or Lorentz) force caused by the local curvature and thickness of the arc [2]. The relative strength between these opposite forces leads to the determination of three characteristic

modes of operation of DC plasma torches [3-7]: steady mode, characterized by a slow or negligible movement of the arc; takeover mode, by a quasiperiodic movement; and restrike mode, by a chaotic movement with sudden and large voltage fluctuations.

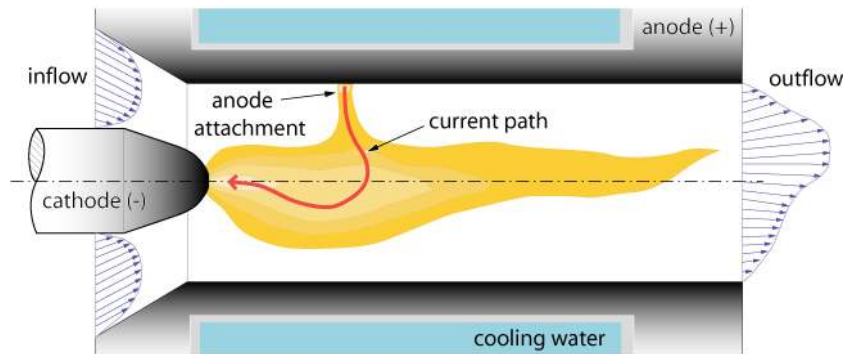


Figure 1: Flow inside a DC non-transferred arc plasma torch.

The strong radiating nature of the arc, added to its confinement inside the torch, has prevented the direct observation of the complete arc dynamics. This has motivated the use of computational models to describe the behavior of the arc inside the torch. The modeling of the arc in DC plasma torches is very challenging because, despite the axisymmetry of the geometry and boundary conditions, the flow is inherently unsteady and three-dimensional; furthermore the flow is highly nonlinear, with large gradients, and spans over a wide range of time and spatial scales. In addition, chemical and thermodynamic non-equilibrium effects have to be considered, especially near the boundaries of the plasma. The first simulations of the arc dynamics were performed by Baudry *et al* [8, 9] using the code ESTET. They simulated the reattachment process by specifying a maximum electric field as control parameter and introducing an artificial hot column at a prespecified position upstream, simulating the formation of a new attachment. Recently, Colombo and Ghedini [10], using the commercial software FLUENT, simulated the plasma flow in a DC torch for a low current and flow rate. An adequate model should capture naturally, at least partially, the different modes of operation of the torch. Such a model has not been reported yet. In this paper we present simulation results of an LTE model of the flow inside three different plasma torches. Our model is capable of describing the steady and takeover modes of operation of the torch without any further assumption on the reattachment process except for the use of an artificially high electrical conductivity near the electrodes, needed because of the equilibrium assumption.

## Mathematical Model

### Model Assumptions

The continuum assumption is valid and the plasma is considered as a compressible, perfect gas in Local Thermodynamic Equilibrium (LTE), hence characterized by a single temperature  $T$  for all its species (atoms, ions, electrons, molecules); the quasi-neutrality condition holds; the plasma is optically thin; Hall currents, gravitational effects, and viscous dissipation are considered negligible.

### Governing Equations

As the plasma is a conducting fluid, its description requires the solution of the fluid conservation and electromagnetic equations; which, according to the assumptions stated above, are given by:

$$\frac{\partial \rho}{\partial t} + \nabla \cdot \rho \vec{u} = 0 \quad (1)$$

$$\rho \left( \frac{\partial \vec{u}}{\partial t} + \vec{u} \cdot \nabla \vec{u} \right) = -\nabla p - \nabla \cdot \vec{\tau} + \vec{j} \times \vec{B} \quad (2)$$

$$\rho C_p \left( \frac{\partial T}{\partial t} + \vec{u} \cdot \nabla T \right) = \nabla \cdot (\kappa \nabla T) + \vec{j} \cdot \vec{E}' - 4\pi \varepsilon_r + \frac{5}{2} \frac{k_B}{e} \vec{j} \cdot \nabla T - \left( \frac{\partial \ln \rho}{\partial \ln T} \right)_p \frac{Dp}{Dt} \quad (3)$$

$$\nabla \cdot (\sigma \nabla \phi) = 0 \quad (4)$$

$$\nabla^2 \vec{A} = -\mu_0 \vec{j} \quad (5)$$

where  $\rho$  is the fluid density,  $\vec{u}$  velocity,  $p$  pressure,  $\vec{\tau}$  the stress tensor; the term  $\vec{j} \times \vec{B}$  represents the Lorentz force, with  $\vec{j}$  as the current density and  $\vec{B}$  the magnetic field;  $C_p$  is the specific heat at constant pressure,  $T$  temperature,  $\kappa$  thermal conductivity,  $\vec{j} \cdot \vec{E}'$  is the Joule heating term, with  $\vec{E}'$  as the effective electric field ( $\vec{E}' = \vec{E} + \vec{u} \times \vec{B}$ ); the term  $4\pi \varepsilon_r$  represents the volumetric radiation losses, with  $\varepsilon_r$  as the net emission coefficient; the term proportional to  $\vec{j} \cdot \nabla T$  represents the diffusion of electron enthalpy, with  $k_B$  as Boltzmann's constant, and  $e$  as the elementary charge; the last term in equation (3) represents the pressure work (equal to zero in constant density flows), with  $D/Dt$  as the substantial derivative;  $\sigma$  is the electrical conductivity,  $\phi$  the electric potential,  $\vec{A}$  the magnetic vector potential and  $\mu_0$  the permeability of free space. These equations are complemented with appropriate thermodynamic and transport properties and the following relations (with  $\mu$  as the dynamic viscosity, and  $\delta$  the identity tensor):

$$\vec{\tau} = -\mu \left( \nabla \vec{u} + \nabla \vec{u}^T - \frac{2}{3} \nabla \cdot \vec{u} \vec{\delta} \right) \quad (6)$$

$$\nabla \times \vec{A} = \vec{B}, \quad \vec{E} = -\nabla\phi - \frac{\partial \vec{A}}{\partial t}, \quad \text{and} \quad \vec{j} = \sigma \vec{E} \quad (7)$$

### Computational Domain and Boundary Conditions

Figure 2 presents the computational domain of the torches studied, typically used in plasma spraying, as well as the computational mesh used for the simulations.

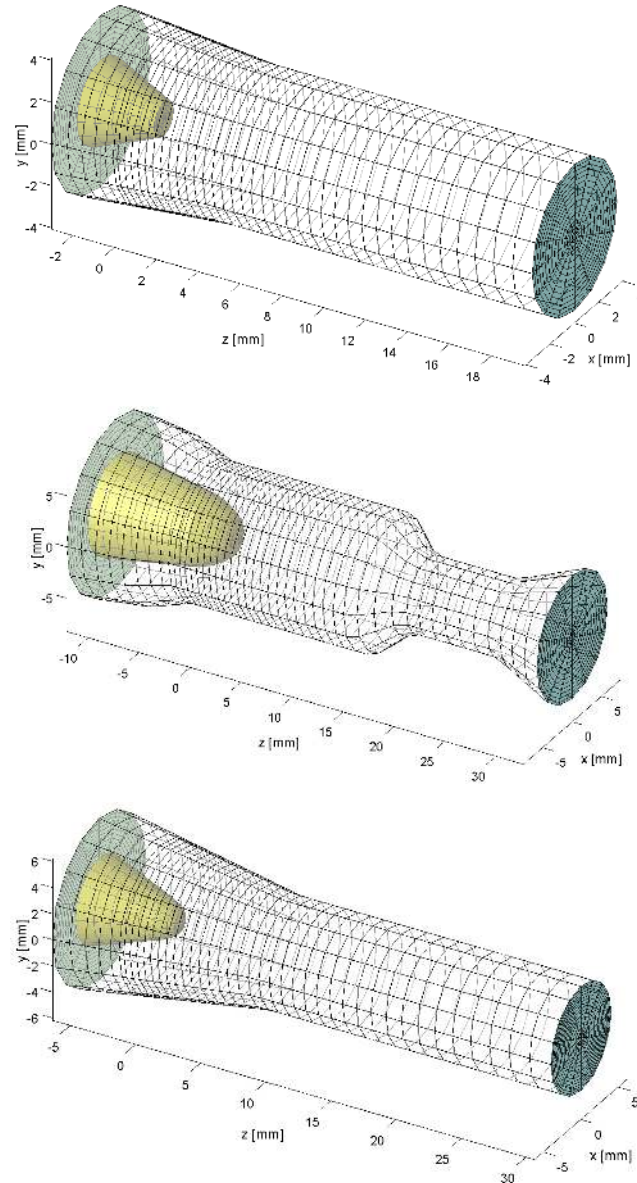


*Figure 2: Geometries studied: (top) torch 1, F4-MB torch from Sulzer-Metco; (center) torch 2 and (bottom) torch 3 SG-100 torch from Praxair with different cathode-anode configurations. Each plot has a different scale; the coordinate axis is centered on the cathode tip .*

To allow the specification of boundary conditions, the boundary of each computational domain is divided in different sides (see Fig. 1). Table 1 shows the boundary conditions used in the simulations, where  $p_0$  represents a reference pressure,  $u_{in}$  the imposed velocity profile (fully developed flow through an annulus),  $T_{in}$  the imposed inlet temperature of 1000 K,  $T_c$  the cathode temperature defined by a Gaussian profile from 1000 to 3600 K at the tip,  $h_w$  the convective heat transfer coefficient at the water cooled anode surface equal to  $10^5$  W/m<sup>2</sup>-K,  $T_w$  a reference cooling water temperature of 500 K, and  $j_c$  the imposed current density over the cathode. A value of  $\sigma$  equal to 8000 1/Ω-m is imposed over the first layer of elements directly in front of the electrodes to allow the passing of the electrical current. This layer of elements has a thickness of ~0.1 mm and mimics the effect of the plasma sheath. Results obtained with a coarser mesh (sheath of ~0.2 mm) produced significantly larger reattachment frequencies, whereas results with a finer mesh (sheath of ~0.05 mm) basically reproduced the same results presented here. However, the use of smaller sheath thickness, a result of the use of better spatial resolution, makes the solution harder to converge due to the sharper gradients near the anode. A more detailed description of the boundary conditions used is found in [12].

Table 1: Boundary conditions.

	$p$	$\bar{u}$	$T$	$\phi$	$\vec{A}$
<b>Side 1: inlet</b>	$p = p_0$	$\bar{u} = \bar{u}_{in}$	$T = T_{in}$	$\phi_{,n} = 0$	$A_i = 0$
<b>Side 2: cathode</b>	$p_{,n} = 0$	$u_i = 0$	$T = T_c$	$\phi_{,n} = 0$	$A_{i,n} = 0$
<b>Side 3: cathode tip</b>	$p_{,n} = 0$	$u_i = 0$	$T = T_c$	$-\sigma\phi_{,n} = j_c$	$A_{i,n} = 0$
<b>Side 4: outlet</b>	$p_{,n} = 0$	$u_{i,n} = 0$	$T_{,n} = 0$	$\phi_{,n} = 0$	$A_i = 0$
<b>Side 5: anode</b>	$p_{,n} = 0$	$u_i = 0$	$-\kappa T_{,n} = h_w(T - T_w)$	$\phi = 0$	$A_{i,n} = 0$

Note:  $y_{,n} = \partial y / \partial n$ ,  $n$  = outer normal to the surface;  $i = x, y, \text{ or } z$

## Numerical Model

Due to the multiscale nature of thermal plasma flows, the equations describing our mathematical model are solved using a Sub-Grid Scale Finite Element Method (SGS-FEM), which separates the solution of a given field into a large scale component (solved over the computational mesh) plus a small or sub-grid scale component (modeled by the method) [11]. The SGS-FEM applied to nonlinear transient advective-diffusive-reactive systems has been implemented in the code *HTPLFLOW* (High

Temperature and *PLasma FLOW* solver) developed in our laboratory. The code is capable to solve an arbitrary number of equations in any number of spatial dimensions on unstructured grids in a fully implicit manner.

## Simulation Results

Table 2 presents the operating conditions of the cases presented here; they were selected to allow the direct comparison of the effects associated with the torch geometry.

*Table 2: Operating conditions for the studied cases.*

	Gas	Current [A]	Flow Rate [slpm]	Injection
Torch 1	Ar-H <sub>2</sub>	600	60	Straight
Torch 2	Ar-H <sub>2</sub>	600	60	Straight
Torch 3a	Ar-H <sub>2</sub>	600	60	Straight
Torch 3b	Ar-H <sub>2</sub>	600	60	Swirl

### Torch 1

This geometry has been studied by Baudry *et al* [8, 9] for the current and flow rate used here, but using swirl injection.

Figure 3 shows a time sequence of the temperature distribution through the vertical plane of the reattachment process. As straight injection is used, it is expected that the arc movement will remain constrained in the vertical plane (plane  $y$ - $z$ , see Fig. 2). As it can be seen, the arc is initially dragged by the incoming flow; then, as the flow pushes the arc downstream, the curvature of the arc increases, increasing the magnetic forces on the arc, and pushing the arc to form a new attachment at the opposite side in the  $y$ -direction of the original attachment. Once a new attachment is formed, the arc first moves upstream until the drag by the incoming flow pushes it downstream again, starting a new reattachment cycle. This behavior of the arc has been determined by our previous simulations and is explained with greater detail in [12].

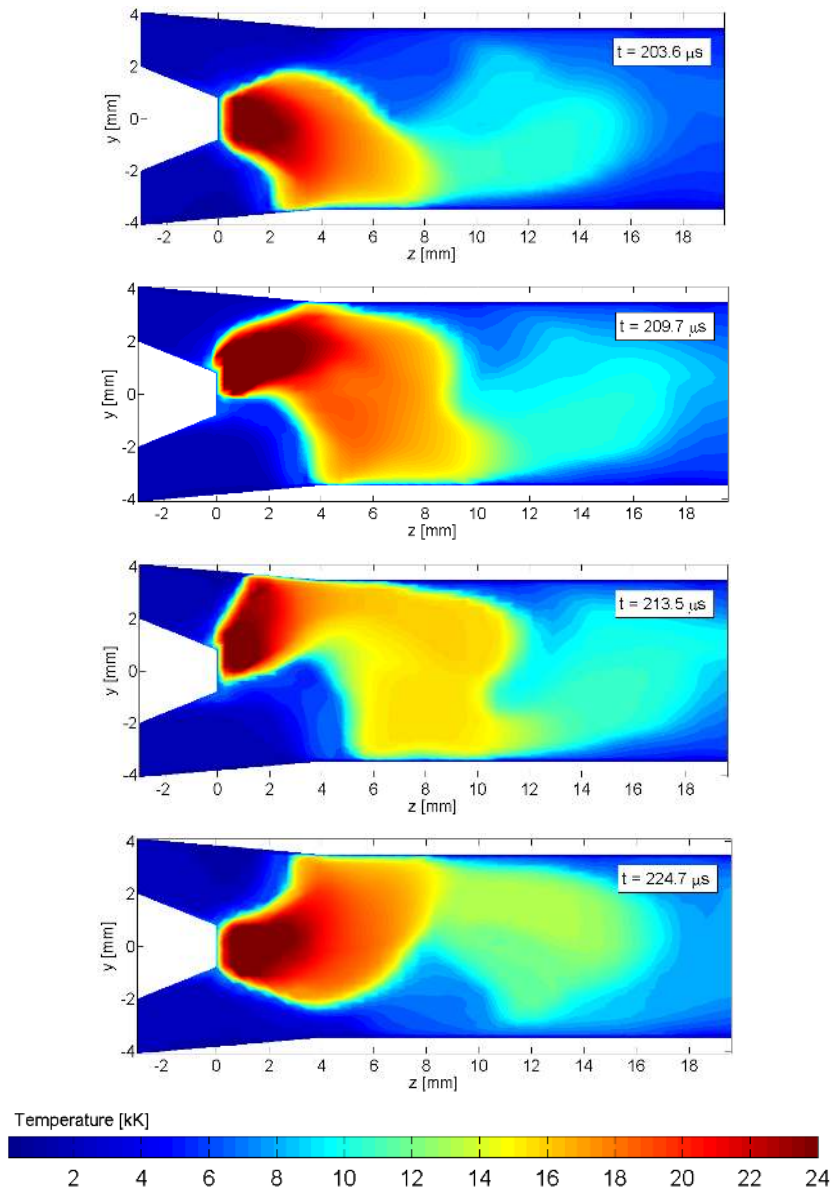


Figure 3: Reattachment process in torch 1 (*T* vertical plane).

### Torch 2

The geometry of torch 2 is significantly different from torch 1 as it presents a sudden constriction of the anode, a much larger diameter and a larger and more rounded cathode tip.

Figure 4 shows a time sequence of the reattachment process for this torch. It can be observed that the constriction of the anode downstream limits the axial movement of the arc. The highest temperatures are observed when the arc is centered on axis.

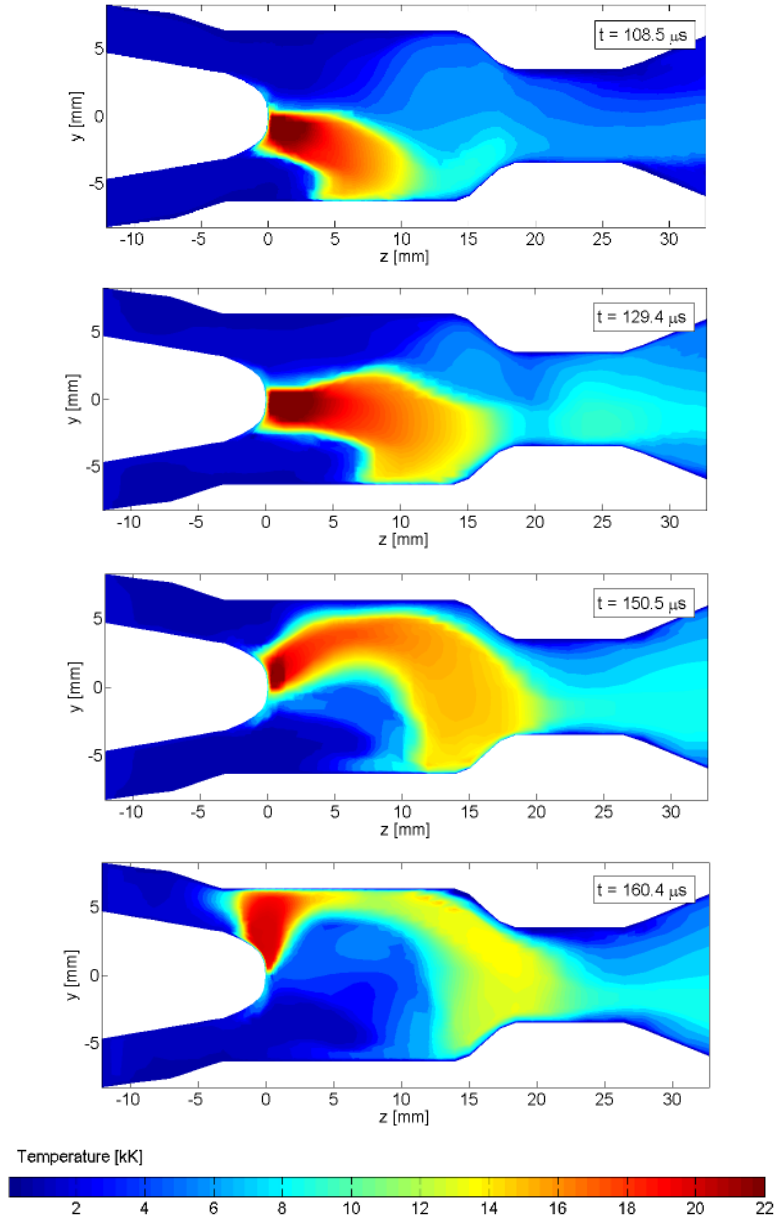


Figure 4: Reattachment process in torch 2 ( $T$  vertical plane).

### Torch 3

Figure 5 shows a time sequence of the reattachment process for torch 3a. Even though, because of the scale of the figure, the arc seems shorter than for torch 1, it is actually longer (the position of the anode attachment is at approximately 5 mm downstream from the cathode tip, whereas for torch 1 this distance is  $\sim 4$  mm). It can also be observed that the arc in this geometry is less robust than the one in torch 1. These characteristics are results of the weaker acceleration experienced by the flow as it



enters the region downstream of the cathode, which has a larger diameter than its counterpart in torch 1 (8 vs. 7 mm).

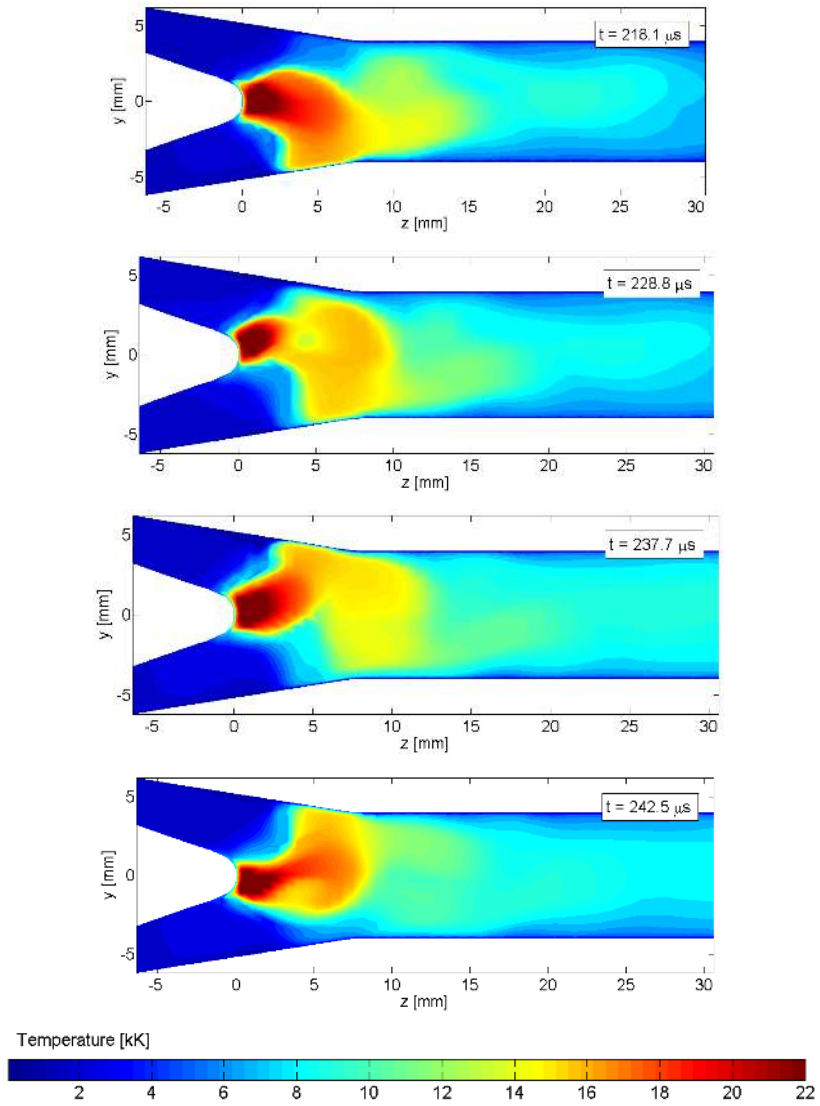
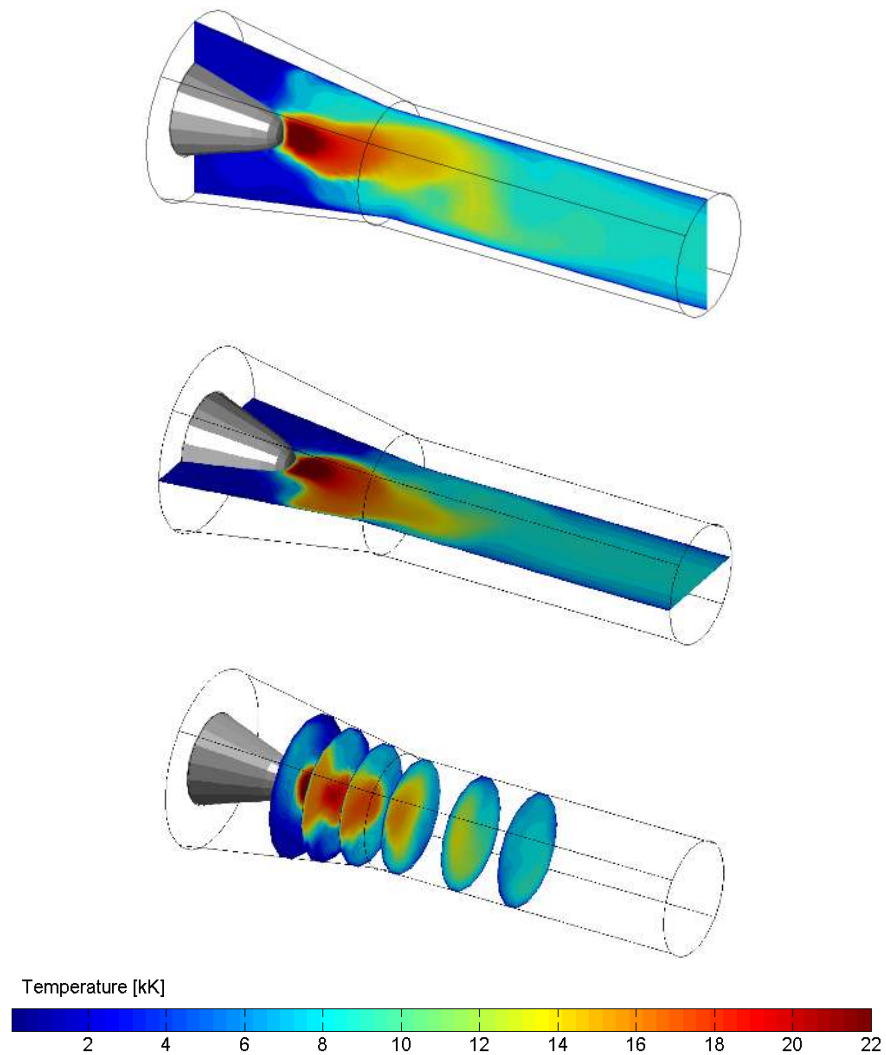


Figure 5: Reattachment process in torch 3a ( $T$  vertical plane).

In Fig. 6 can be observed the temperature distribution inside the torch when swirl injection is used (torch 3b); the three-dimensionality of the flow is clearly observed. From these results, it is clear that the arc cannot be described adequately by a two dimensional nor by a steady-state model.

This three-dimensionality does not allow us to present a reattachment sequence for torch 3b in plots similar to the previous figures. A sequence of the reattachment process is shown in Fig. 7. In Fig. 7, between the top and the center figure, the anode attachment is dragged axially and circumferentially

counterclockwise with respect to the  $z$  axis, following a helix. In the center figure, the beginning of the formation of a new attachment can be observed at almost the opposite side of the original attachment. This new attachment becomes dominant, completing the reattachment process, and leaving the arc in the position shown in the bottom figure, completing a reattachment cycle. The new arc then starts being dragged by the flow and a new cycle initiates.



*Figure 6: Temperature distribution through vertical, horizontal, and axially distributed cross sections for torch 3b.*

This behavior of the arc is explained as follows: As the arc is dragged around the anode surface, it lengthens, its curvature increases, which produces an increase of the magnetic forces acting on it, pushing the arc to the opposite side of the attachment and leading to the formation of a new

attachment, almost at the opposite side of the original one. This behavior has been observed experimentally in our laboratory by the use of end-on imaging of the arc and has been reported in [4].

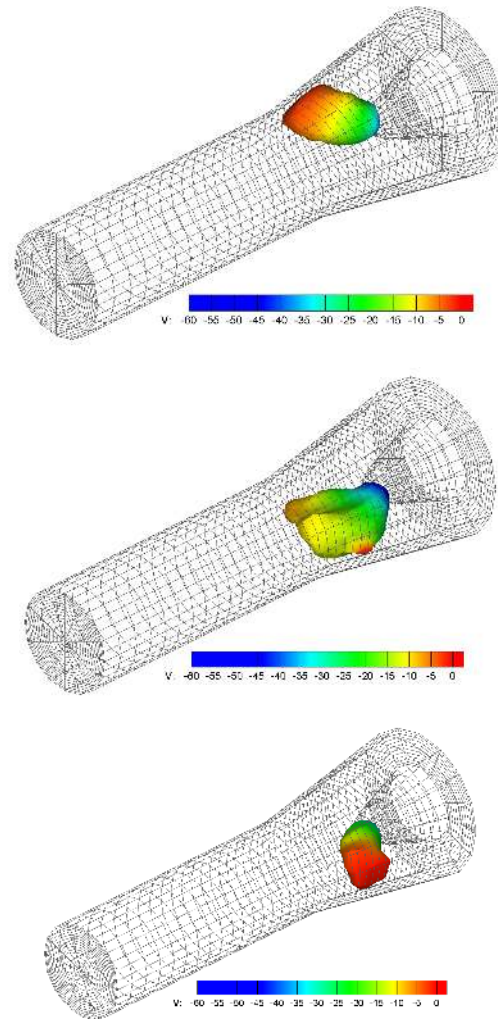


*Figure 7: Time sequence of reattachment process) for torch 3b; electric potential distribution over the 14000 K isosurface (representing the shape of the arc).*

### Time Dependent Characteristics and Frequency Analysis

As the voltage drop is proportional to the arc length, the movement of the arc is reflected by the voltage drop signal, which is strongly correlated to other characteristics of the flow inside the torch, like the maximum and average temperatures, velocities, and pressure drop. Voltage traces of the cases simulated as well as experimental results from [14] are presented in Fig. 8, where the rectangle in the bottom figure indicates approximately the time scale of the simulation results shown. Despite the conditions of the experimental results (SG-100 torch, 700A, Ar 63 slpm, H<sub>2</sub> 5 slpm) do not match the

conditions used in our simulations, they are close to the conditions of torch 3b. As expected, the greater percentage of  $H_2$  used in torch 3b causes a larger reattachment frequency and a larger voltage drop. The cases studied here have had Bauldry’s simulations as base case. We are currently in the process of comparing our results with experimental data. The frequency analysis of the total voltage drop over time obtained from our simulations allows the determination of the main reattachment periods and frequencies of the plasma flow. These characteristics allow a more direct comparison with experimental measurements, as the analysis of the voltage signal is commonly used as a parameter for the determination of the characteristics of the arc under given operating conditions. Table 3 summarizes the reattachment periods and frequencies, as well as the time-averaged average axial velocity and temperature at the outlet obtained from our simulations. The effect of the anode diameter can be clearly deduced from this table: as the diameter is increased, the reattachment frequency is decreased. Furthermore, the effect of the constriction of the anode in torch 2 evidences the lengthening of the reattachment period. The obtained frequencies are so far typically a factor from 2 to 4 larger than the ones obtained experimentally. Moreover, the obtained velocities and temperatures at the outlet are 30 to 40% smaller than the ones measured. We expect that the use of better spatial resolution in our simulations, as well as the use of a non-equilibrium model will allow better agreement with experiments.

*Table 3: Predicted reattachment periods and frequencies, and time averaged mean velocity and temperature at the outlet.*

	Reattachment Period [ $\mu$ s]	Reattachment Frequency [kHz]	Mean Velocity at Outlet [m/s]	Mean Temperature at Outlet [K]
Torch 1	48.3	20.7	498	5240
Torch 2	85.2	11.7	547	4460
Torch 3a	19.7	50.7	345	4087
Torch 3b	27.0	37.0	317	4023

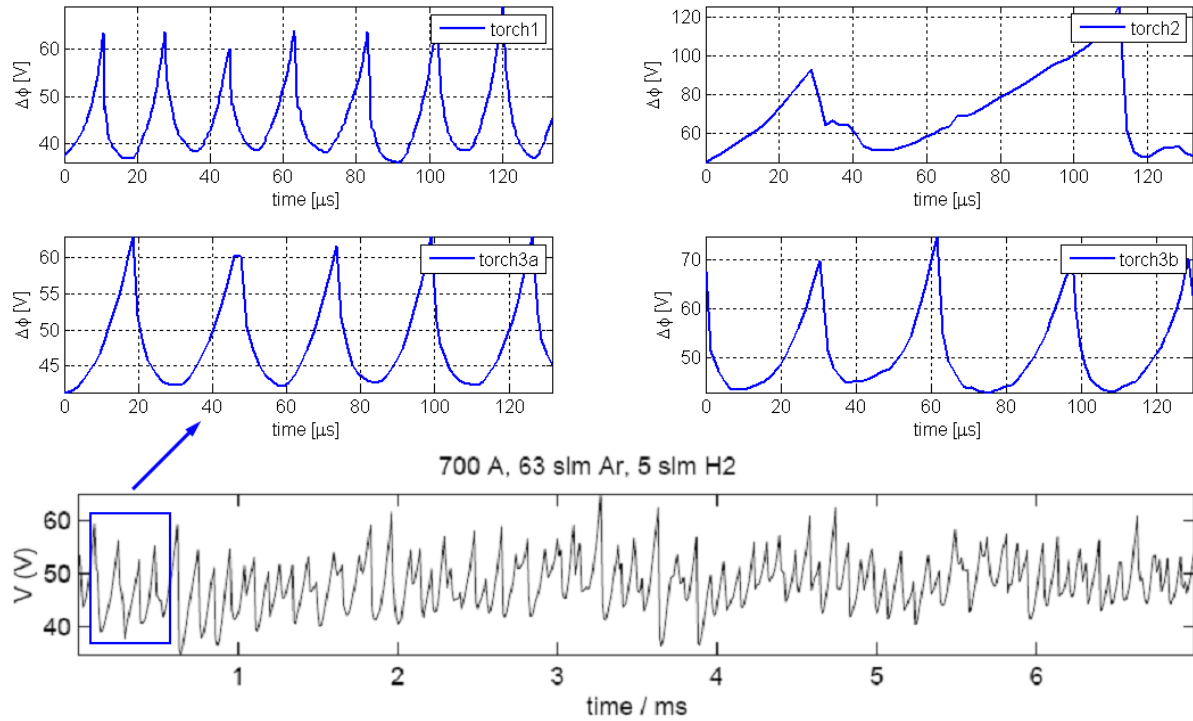


Figure 8: Voltage traces for the torches simulated and experimental voltage trace reported in [14].

## Conclusions

Three-dimensional, transient simulations of three different torch geometries have been performed to study the behavior of the arc inside plasma spraying torches. It has been observed that, when swirl or straight injection is used, the arc will initially be dragged by the incoming flow and then will reattach preferably at the opposite side of its original attachment. This phenomenon, observed experimentally, seems to be caused primary by the imbalance between drag and electromagnetic forces. Even though the obtained reattachment frequencies obtained by our model are at present a factor between 2 to 4 larger than the experimental ones, the model can be used as a tool for the design plasma spraying torches.

## Acknowledgments

This research has been supported by NSF Grant CTS-0225962. Computing time from a grant from the University of Minnesota Supercomputing Institute (MSI) is gratefully acknowledged. We especially thank Shuxia Zhang from the MSI for her help in the implementation of our code.

## References

1. E. Pfender, Thermal Plasma Technology: Where Do We Stand and Where Are We Going?, *Plasma Chem. Plasma Proc.*, Vol. 19 (No. 1), 1999, p. 1-31
2. S.A. Wutzke, "Conditions Governing the Symptomatic Behavior of an Electric Arc in a Superimposed Flow Field", Ph.D. Thesis, University of Minnesota, 1967
3. Z. Duan, J. Heberlein, S. Janisson, K. Wittmann, J.F. Coudert and P. Fauchais, Effects of Nozzle Fluid Dynamics on the Dynamic Characteristics of a Plasma Spray Torch, *United Thermal Spray Conf., Tagungsband*, E. Lugscheider and P.A. Kammer, Ed., 1999, p. 247-252.
4. Z. Duan, "Investigations of Plasma Instabilities in a Spray Torch", Ph.D. Thesis, University of Minnesota, 2000
5. Z. Duan and J.V.R. Heberlein, Arc Instabilities in a Plasma Spray Torch, *J. Therm. Spray Technol.*, Vol 11 (No. 1), 2002, p. 44-51
6. J.F. Coudert and P. Fauchais, Arc Instabilities in a D.C. Plasma Torch, *High Temp. Material Processes*, Vol. 1, 1997, p. 149-166
7. J.F. Coudert, M.P. Planche, and P. Fauchais, Characterization of D.C. Plasma Torch Voltage Fluctuations, *Plasma Chem. Plasma Proc.*, Vol. 16 (No. 1), 1996, p. 211s-227s
8. C. Baudry, A. Vardelle, and G. Mariaux, Numerical Modeling of a DC Non-Transferred Plasma Torch: Movement of the Arc Anode Attachment and Resulting Anode Erosion, *High Tech. Plasma Proc.*, Vol. 9, 2005, p. 1-15
9. C. Baudry, "Contribution à la Modélisation Instationnaire et Tridimensionnelle du Comportement Dynamique de l'Arc Dans une Torche de Projection Plasma", Doctoral Thesis, Université de Limoges, 2003
10. V. Colombo and E. Ghedini, Time Dependent 3-D Simulation of a DC Non-Transferred Arc Plasma Torch: Anode Attachment and Downstream Region Effects, *Proc. of the 17th Int. Symp. Plasma Chemistry*, 2005, p. 169
11. T.J.R. Hughes, G.R. Feijoo, L. Mazei, and J.B. Quincy, The Variational Multiscale Method - A Paradigm For Computational Mechanics, *Comput. Methods Appl. Mech. Engrg.*, Vol. 166, 1998, p. 3-24
12. J.P. Trelles, E. Pfender, and J.V.R. Heberlein, Multiscale Finite Element Modeling of Arc Dynamics in a DC Plasma Torch, *Plasma Chem. Plasma Proc.*, article in press, 2005

13. He-Ping Li, E Pfender and Xi Chen, Application of Steenbeck's Minimum Principle for Three-Dimensional Modelling of DC Arc Plasma Torches, *J. Phys. D: Appl. Phys.* 36, 2003, p. 1084-1096
14. M. Vysohlid, J. Heberlein, Investigation of Arc Voltage Fluctuations in a Plasma Torch SG-100 operated with Ar/H<sub>2</sub>, Thermal Spray 2004: Advances in Technology and Application, ASM International, May 10-12, 2004 (Osaka, Japan), ASM International, 2004